High-beta equilibria in tokamaks with pressure anisotropy and toroidal flow

B. Layden, M. J. Hole, and R. Ridden-Harper

Citation: Physics of Plasmas **22**, 122513 (2015); doi: 10.1063/1.4939026
View online: http://dx.doi.org/10.1063/1.4939026
View Table of Contents: http://scitation.aip.org/content/aip/journal/pop/22/12?ver=pdfcov
Published by the AIP Publishing

High-beta equilibria in tokamaks with pressure anisotropy and toroidal flow

B. Layden,[a] M. J. Hole, and R. Ridden-Harper
Research School of Physics and Engineering, The Australian National University, Acton, ACT 2601, Australia

(Received 13 July 2015; accepted 14 December 2015; published online 30 December 2015)

We extend previous analytical calculations of 2D high-β equilibria in order-unity aspect ratio tokamaks with toroidal flow to include pressure anisotropy, assuming guiding-center theory for a bi-Maxwellian plasma and the ideal MHD Ohm's law. Equilibrium solutions are obtained in the core region (which fills most of the plasma volume) and the boundary layer. We find that pressure anisotropy with $p_\parallel > p_\perp$ ($p_\parallel < p_\perp$) reduces (enhances) the plasma diamagnetism relative to the isotropic case whenever an equilibrium solution exists. Sufficiently fast toroidal flows ($\Omega > \Omega_{\min}$) were previously found to suppress the field-free region (diamagnetic hole) that exists in static isotropic high-β equilibria. We find that all equilibrium solutions with pressure anisotropy suppress the diamagnetic hole. For the static case with a volume-averaged toroidal beta of 70%, plasmas with max $(p_\parallel/p_\perp) > \alpha_1 = 1.07$ have equilibrium solutions. We find that α_1 decreases with increasing toroidal flow speed, and above the flow threshold $\Omega_{\min}$ we find $\alpha_1 = 1$, so that all $p_\parallel > p_\perp$ plasmas have equilibrium solutions. On the other hand, for $p_\parallel < p_\perp$ there are no equilibrium solutions below $\Omega_{\min}$. Above $\Omega_{\min}$ (where there is no diamagnetic hole in the isotropic case), equilibrium solutions exist for $\alpha_2 < \min(p_\parallel/p_\perp) < 1$, where α_2 decreases from unity with increasing flow speed. The boundary layer width increases and the Shafranov shift decreases for $p_\parallel > p_\perp$, while the converse is true for $p_\parallel < p_\perp$. © *2015 AIP Publishing LLC*. [http://dx.doi.org/10.1063/1.4939026]

I. INTRODUCTION

Increasingly high values of $\beta \equiv 2\mu_0 p/B^2$ are being obtained in modern high-performance tokamaks, offering enhanced thermal fusion power output.[1] Volume-averaged toroidal betas of 40% have been achieved on the START[2] and NSTX[3] spherical tokamaks, and volume-averaged toroidal betas of 30%, 50%, and 60% are projected for the proposed Component Test Facility[4] (CTF), ARIES-ST,[5] and Spherical Tokamak Power Plant[6] (STPP), respectively. Physical models of these devices must allow for these high β values as well as inverse aspect ratios $\epsilon \equiv a/R_0$ of order unity to give accurate descriptions of their behavior.

Modern tokamaks rely critically on auxiliary heating methods such as ion cyclotron resonance heating (ICRH) and neutral beam injection (NBI) which generate significant pressure anisotropy in the plasma, the latter also driving strong plasma flows. Both pressure anisotropy and flow can significantly modify the force balance in the plasma and lead to pressure, density, and current surfaces that no longer coincide with magnetic surfaces.[7–12] The inclusion of pressure anisotropy and flow is therefore crucial for studies of equilibria in experiments with auxiliary heating.

Analytical studies for small[13] and unity[14,15] inverse aspect ratios have shown fundamental changes to equilibria at high β, defined by the ordering $\beta \gg \epsilon^2/q^2$ where q is the safety factor. The equilibrium solution separates into two asymptotic regions: the core region where the poloidal flux ψ is a function of the major radius only (giving vertical flux contours), and a narrow boundary layer region adjoining the conducting wall in which the flux surfaces close (see Fig. 1). This leads to a large outward shift of the magnetic axis (i.e., Shafranov shift). These analytical high-β solutions have been confirmed with numerical high-β Grad-Shafranov solvers.[16]

The most striking feature of high-β equilibria solutions is the existence of a magnetic field-free region, called a diamagnetic hole, above a critical β.[13–15] In this region, there are no physical solutions of the Grad-Shafranov equation. In a recent work, Fitzgerald *et al.*[15] analyzed the effect of toroidal flow on these high-β equilibrium solutions in order-unity aspect ratio tokamaks. Toroidal flow was found to reduce the plasma diamagnetism, and even completely suppress the diamagnetic hole above a critical flow speed. The combined effect of toroidal flow and pressure anisotropy on high-β equilibria, however, has yet to be studied.

We extend the work of Fitzgerald *et al.*[15] in this paper to include both pressure anisotropy and toroidal flow in the analytical study of high-β equilibria. Starting our analysis from a modified Grad-Shafranov equation for plasmas with pressure anisotropy and toroidal flow, we solve for the equilibrium in the core and boundary layer. We then investigate the character of the solutions for different levels of pressure anisotropy and flow speeds.

II. THEORETICAL BACKGROUND

We begin our analysis assuming the guiding-center plasma (GCP) model[17–19] for a two-temperature anisotropic plasma and the ideal MHD Ohm's law. The equations for plasma equilibrium in this model are

$$\rho \boldsymbol{u} \cdot \nabla \boldsymbol{u} = -\nabla \cdot \mathbf{P} + \boldsymbol{J} \times \boldsymbol{B}, \tag{1}$$

$$\nabla \times \boldsymbol{B} = \mu_0 \boldsymbol{J}, \tag{2}$$

$$\nabla \cdot \boldsymbol{B} = 0, \tag{3}$$

[a]Electronic mail: brett.layden@anu.edu.au

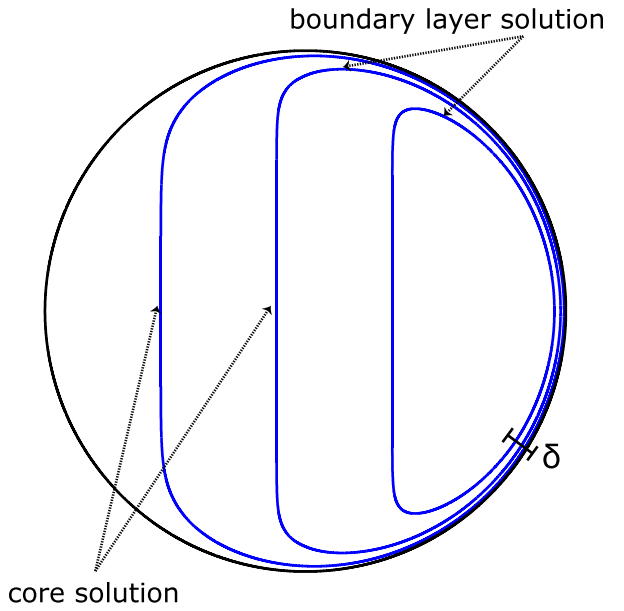

FIG. 1. Contours of constant poloidal magnetic flux ψ given by the analytical solution for high-β equilibrium. The core and boundary layer solutions are solved separately then joined; δ is the width of the boundary layer.

$$\nabla \times \boldsymbol{E} = 0, \tag{4}$$

$$\boldsymbol{E} + \boldsymbol{u} \times \boldsymbol{B} = 0, \tag{5}$$

and

$$\mathbf{P} = p_\perp \mathbf{I} + \frac{\Delta \boldsymbol{B}\boldsymbol{B}}{\mu_0}, \tag{6}$$

where

$$\Delta \equiv \mu_0 \frac{p_\parallel - p_\perp}{B^2}. \tag{7}$$

Here, ρ is the single-fluid mass density, $\boldsymbol{u}$ is the single-fluid velocity, and $\mathbf{P}$ is the single-fluid pressure tensor with components $p_\parallel$ and $p_\perp$ parallel and perpendicular to the magnetic field, respectively, with $\mathbf{I}$ the identity tensor. Equation (1) is the GCP force balance equation, Eqs. (2)–(4) are Maxwell's equations, and Eq. (5) is the ideal Ohm's law.

For anisotropic plasmas, the boundary-value equilibrium problem is well posed only if the inequalities

$$1 - \Delta > 0 \tag{8}$$

and

$$1 + \frac{\mu_0}{B}\frac{\partial p_\perp}{\partial B} > 0 \tag{9}$$

are satisfied everywhere, so the inequalities are therefore necessary conditions for equilibrium existence;[17,18] these inequalities may be violated when $p_\parallel > p_\perp$ and $p_\parallel < p_\perp$, respectively. Equations (8) and (9) also correspond to conditions for dynamical stability to localized disturbances,[17,18] in which context they are, respectively, called the firehose and mirror stability conditions. Although the focus of this paper is on the equilibrium problem, for convenience we henceforth refer to Eqs. (8) and (9) as the "firehose" and "mirror" conditions for equilibrium existence. The mirror condition may also be stated as[20]

$$\tilde{\beta} \equiv \frac{\beta_\perp^2}{\beta_\parallel} - \beta_\perp < 1, \tag{10}$$

where

$$\beta_{\parallel,\perp} \equiv \frac{2\mu_0 p_{\parallel,\perp}}{B^2}. \tag{11}$$

Since $\boldsymbol{B}$ is a divergence-less vector field, it can be written in an axisymmetric coordinate system (R, ϕ, Z) as[21]

$$\boldsymbol{B} = \nabla\psi \times \nabla\phi + RB_\phi \nabla\phi, \tag{12}$$

where ψ is the poloidal magnetic flux, B_ϕ is the magnitude of the toroidal magnetic field, and where $\nabla\psi \times \nabla\phi$ gives the poloidal magnetic field $\boldsymbol{B}_\theta$. If the plasma flow is purely toroidal then, using $\nabla \times (\boldsymbol{u} \times \boldsymbol{B}) = 0$ from Eqs. (4) and (5), the fluid velocity can be written as

$$\boldsymbol{u} = R^2 \Omega(\psi) \nabla\phi, \tag{13}$$

where the toroidal angular velocity $\Omega(\psi)$ is a free flux function.

We now outline the derivation of the Grad-Shafranov equation for an anisotropic plasma with toroidal flow (see, e.g., Refs. 7, 8, and 10). Taking the $\nabla\phi$ component of Eq. (1) and substituting Eq. (12) yields

$$RB_\phi = \frac{F(\psi)}{(1-\Delta)}, \tag{14}$$

where $F(\psi)$ is a free flux function. The $\boldsymbol{B}$ component of Eq. (1) gives the Bernoulli equation

$$W(\rho, B, \psi) - \frac{R^2\Omega^2(\psi)}{2} = H(\psi), \tag{15}$$

where $H(\psi)$ is a free flux function and W is the enthalpy. To close the set of equations, we assume a bi-Maxwellian distribution in which the temperature parallel to the magnetic field, $T_\parallel$, is constant on flux surfaces so that $T_\parallel = T_\parallel(\psi)$. The perpendicular temperature in this model is given by[7,10]

$$T_\perp(B, \psi) = \frac{BT_\parallel(\psi)}{B - T_\parallel(\psi)\Theta(\psi)}, \tag{16}$$

where $\Theta(\psi)$ is a free flux function that measures the degree of temperature anisotropy; $\Theta < 0$ ($\Theta > 0$) corresponds to $T_\parallel > T_\perp$ ($T_\parallel < T_\perp$). The parallel and perpendicular pressures are then given by

$$p_\parallel(\rho, B, \psi) = \frac{\rho k T_\parallel(\psi)}{m} \tag{17}$$

and

$$p_\perp(\rho, B, \psi) = \frac{\rho k T_\perp(B, \psi)}{m}. \tag{18}$$

The enthalpy W in this model is given (to within a gauge transformation) by[7,10]

$$W(\rho,B,\psi)=\frac{kT_\parallel(\psi)}{m}\log\left(\frac{\rho}{\rho_0}\frac{T_\parallel(\psi)}{T_\perp(B,\psi)}\right), \tag{19}$$

where ρ_0 is an arbitrary constant. Equations (15) and (19) imply that the mass density can be expressed as

$$\rho(R,B,\psi)=\frac{T_\perp(B,\psi)}{T_\parallel(\psi)}\bar{K}(\psi)\exp\left(\frac{mR^2\Omega^2(\psi)}{2kT_\parallel(\psi)}\right), \tag{20}$$

where

$$\bar{K}(\psi)=\rho_0\exp\left(\frac{mH(\psi)}{kT_\parallel(\psi)}\right). \tag{21}$$

Finally, taking the $\nabla\psi$ component of Eq. (1) gives the modified Grad-Shafranov equation

$$\Delta^*\psi\equiv R^2\nabla\cdot\left[(1-\Delta)\frac{\nabla\psi}{R^2}\right]=\mu_0RJ_\phi, \tag{22}$$

where

$$RJ_\phi(R,\psi)=-\frac{FF'}{\mu_0(1-\Delta)}-R^2\rho\left[H'+\frac{kT_\parallel'}{m}-\left(\frac{\partial W}{\partial\psi}\right)_{\rho,B}-R^2\Omega\Omega'\right], \tag{23}$$

with J_ϕ the toroidal current density (where the function arguments in Eq. (23) are omitted for brevity). Writing the enthalpy term in Eq. (23) explicitly gives

$$\left(\frac{\partial W}{\partial\psi}\right)_{\rho,B}=\frac{k}{m}\left[T_\parallel'\log\left(\frac{\rho}{\rho_0}\frac{T_\parallel}{T_\perp}\right)-\frac{T_\perp\left(T_\parallel\Theta'+T_\parallel'\Theta\right)}{B}\right]. \tag{24}$$

Thus, the equilibrium configuration is determined by five free flux functions: $\Omega(\psi),F(\psi),T_\parallel(\psi),H(\psi)$, and $\Theta(\psi)$.

III. QUALITATIVE EQUILIBRIUM PROPERTIES

A. Ordering

We can deduce properties of the high-beta equilibrium solution by first examining the force balance equation. We rewrite Eq. (1) as

$$\rho\boldsymbol{u}\cdot\nabla\boldsymbol{u}=-\nabla\cdot\mathbf{P}-\frac{\nabla B_\phi^2}{2\mu_0}-\frac{\nabla B_\theta^2}{2\mu_0}-\frac{B_\phi^2}{\mu_0}\frac{\nabla R}{R}+\frac{\boldsymbol{B}_\theta\cdot\nabla\boldsymbol{B}_\theta}{\mu_0}. \tag{25}$$

In terms of the inverse aspect ratio $\epsilon=r/R\sim1$, where r and R are, respectively, the minor radius and major radius, the safety factor q can be approximated as

$$q=O\left(\epsilon\frac{B_\phi}{B_\theta}\right). \tag{26}$$

We also make the estimates

$$\rho\boldsymbol{u}\cdot\nabla\boldsymbol{u}=-\rho u_\phi^2\frac{\nabla R}{R}=O\left(\epsilon\rho u_\phi^2\right) \tag{27}$$

and

$$\beta_{\parallel,\perp}=O\left(\frac{\mu_0p_{\parallel,\perp}}{B_\phi^2}\right), \tag{28}$$

where u_ϕ is the toroidal flow speed $R\Omega(\psi)$, and we introduce the Alfvén Mach number M_ϕ through the equation

$$\rho u_\phi^2=\frac{M_\phi^2B_\phi^2}{\mu_0}. \tag{29}$$

We assume that $\beta_\parallel\sim\beta_\perp$ and let β denote their order of magnitude. Ordering Eq. (25) against B_ϕ^2/μ_0 in terms of the dimensionless quantities yields

$$\underbrace{\rho\boldsymbol{u}\cdot\nabla\boldsymbol{u}}_{O\left(\epsilon M_\phi^2\right)}=\underbrace{-\nabla\cdot\mathbf{P}}_{O(\beta)}\underbrace{-\frac{\nabla B_\phi^2}{2\mu_0}}_{O(1)}\underbrace{-\frac{\nabla B_\theta^2}{2\mu_0}}_{O\left(\epsilon^2/q^2\right)}\underbrace{-\frac{B_\phi^2}{\mu_0}\frac{\nabla R}{R}}_{O(\epsilon)}+\underbrace{\frac{\boldsymbol{B}_\theta\cdot\nabla\boldsymbol{B}_\theta}{\mu_0}}_{O\left(\epsilon^2/q^2\right)}. \tag{30}$$

B. Core and boundary regions

We first consider the core region, where the toroidal field terms and the toroidal flow term in Eq. (30) dominate over the poloidal field terms, owing to the high-β and fast-flow orderings $\beta q^2\gg\epsilon^2$ and $M_\phi^2q^2\gg\epsilon$, respectively. Equation (30) then becomes

$$\rho\boldsymbol{u}\cdot\nabla\boldsymbol{u}=-\nabla\cdot\mathbf{P}-\frac{\nabla B_\phi^2}{2\mu_0}-\frac{B_\phi^2}{\mu_0}\frac{\nabla R}{R}. \tag{31}$$

Combining $\beta q^2\gg\epsilon^2$ with Eq. (26) yields $B_\theta/B_\phi\ll\sqrt{\beta}$, so we can neglect B_θ in the core for our high-β solutions. Therefore, we set $B=B_\phi$ in Eqs. (7) and (16). Then, substituting Eqs. (7), (16)–(18), and (20) into Eq. (14), we derive a cubic equation for B_ϕ

$$0=[RB_\phi-F(\psi)][B_\phi-T_\parallel(\psi)\Theta(\psi)]^2+RT_\parallel^2(\psi)\times\Theta(\psi)Y(R,\psi), \tag{32}$$

where

$$Y(R,\psi)\equiv\frac{\mu_0k}{m}\bar{K}(\psi)\exp\left(\frac{mR^2\Omega^2(\psi)}{2kT_\parallel(\psi)}\right). \tag{33}$$

Therefore, the solutions of Eq. (32) satisfy $B_\phi=B_\phi(R,\psi)$ in the core. Substituting $B_\phi=B_\phi(R,\psi)$ back into the equations for the other variables implies, sequentially, that $T_\perp=T_\perp(R,\psi)$, $\rho=\rho(R,\psi)$, $p_{\parallel,\perp}=p_{\parallel,\perp}(R,\psi)$, and $\mathbf{P}=\mathbf{P}(R,\psi)$. Writing

$$\boldsymbol{u}_\phi \cdot \nabla \boldsymbol{u}_\phi = -\frac{u_\phi^2}{R}\nabla R = -R\Omega^2(\psi)\nabla R, \tag{34}$$

it can be seen from Eq. (31) that $\psi = \psi(R)$ in the core; so, in this region, contours of constant ψ are vertical lines. This result was also found for static[13,14] and flowing[15] isotropic high-β equilibria.

The assumption of closed flux surfaces necessitates that the poloidal field terms in Eq. (30) become significant outside the core region; this implies the existence of a boundary layer in which $\nabla\psi$ is large and the flux surfaces close,[13–15] as shown in Fig. 1. This boundary layer is located at large R, where the poloidal field forces must compensate the weaker toroidal field forces to maintain equilibrium. The width of the boundary layer δ is determined by balancing the unbalanced part of the centrifugal, pressure, and toroidal field forces with the poloidal field force. For static isotropic equilibria the width was found to be $\delta/r = O(\sqrt{\epsilon/\beta q^2})$.[14]

IV. ANALYTICAL SOLUTION

A. Core

Assuming that $\beta q^2 \gg \epsilon^2$ in the core region, the Grad-Shafranov operator $\Delta^*\psi$ can be neglected to lowest order.[14] Then, Eq. (22) becomes

$$0 = -\frac{F(\psi)F'(\psi)}{\mu_0(1-\Delta)} - R^2\rho(R,B,\psi) \times \left[H'(\psi) + \frac{kT_\parallel'(\psi)}{m} - \left(\frac{\partial W}{\partial \psi}\right)_{\rho,B} - R^2\Omega(\psi)\Omega'(\psi)\right]. \tag{35}$$

As by Fitzgerald *et al.*,[15] we simplify the solution by introducing a new spatial variable $X(\psi)$ defined implicitly by

$$0 = XJ_{c\phi}(X), \tag{36}$$

with

$$XJ_{c\phi}(X) \equiv -\frac{F(X)F'(X)}{\mu_0[1-\Delta(B_\phi,X)]} - X^2\rho_c(B_\phi,X) \times \left[H'(X) + \frac{kT_\parallel'(X)}{m} - \left(\frac{\partial W}{\partial X}\right)_{\rho_c,B_\phi} - X^2\Omega(X)\Omega'(X)\right], \tag{37}$$

$$\rho_c(B_\phi,X) \equiv \frac{T_\perp(B_\phi,X)}{T_\parallel(X)}\rho_i(X), \tag{38}$$

and

$$\rho_i(X) \equiv \bar{K}(X)\exp\left(\frac{mX^2\Omega^2(X)}{2kT_\parallel(X)}\right), \tag{39}$$

and where $B_\phi(X)$ is a solution of

$$0 = [XB_\phi - F(X)][B_\phi - T_\parallel(X)\Theta(X)]^2 + XT_\parallel^2(X) \times \Theta(X)Y(X), \tag{40}$$

with

$$Y(X) \equiv \frac{\mu_0 k}{m}\rho_i(X). \tag{41}$$

Comparing Eqs. (37)–(41) with Eqs. (20), (32), and (35), we see that $R = X(\psi)$ in the core by construction, and Eqs. (38) and (40) give the mass density and toroidal magnetic field as functions of radial position in the core. The mass density ρ_c is equal to ρ_i if the temperature is isotropic. Also, we note that the free poloidal flux functions are now specified in terms of new free functions of X.

In order to obtain a consistent solution of Eq. (36) we must specify 4 of the 5 free functions of X and solve for the remaining free function. We choose to solve Eq. (36) for $F(X)$ in terms of the other 4 free functions. However, before proceeding, we make $\rho_i(X)$ a free function in place of $H(X)$ since $\rho_i(X)$ is more closely related to a directly measurable quantity (i.e., the mass density). By rewriting Eq. (20), the subsidiary quantity $H(X)$ is related to $\rho_i(X)$ by

$$H(X) = \frac{kT_\parallel(X)}{m}\log\left(\frac{\rho_i(X)}{\rho_0}\right) - \frac{1}{2}X^2\Omega^2(X), \tag{42}$$

which leads to

$$H'(X) = \frac{k}{m}\left[T_\parallel\frac{\rho_i'}{\rho_i} + T_\parallel'\log\left(\frac{\rho_i}{\rho_0}\right)\right] - X\Omega^2 - X^2\Omega\Omega', \tag{43}$$

where the prime now refers to differentiation with respect to X. We note that the mass density in the boundary layer $\rho(R,X)$ is related to $\rho_i(X)$ by

$$\rho(R,X) = \frac{T_\perp(B,X)}{T_\parallel(X)}\rho_i(X)\exp\left(\frac{m(R^2-X^2)\Omega^2(X)}{2kT_\parallel(X)}\right). \tag{44}$$

Writing $FF' = d(F^2/2)/dX$ then rearranging Eq. (36) and integrating, we have

$$F(X) = \sqrt{F(R_{\min})^2 - 2\mu_0\int_{R_{\min}}^{X} dX'\,\Gamma(X')}, \tag{45}$$

where

$$\Gamma(X) \equiv -(1-\Delta)X^2\rho_c\left[H' + \frac{kT_\parallel'}{m} - \left(\frac{\partial W}{\partial X}\right)_{\rho_c,B_\phi} - X^2\Omega\Omega'\right], \tag{46}$$

with $R_{\min}$ the location of the inboard boundary along the major axis and $F(R_{\min})$ a free parameter that determines B_ϕ at the inboard boundary. Both sides of Eq. (45) depend on F, since B_ϕ appears in $\Gamma(X)$ and depends on F through Eq. (40). We therefore solve Eq. (45) recursively. We assume an initial function $F(X) = F_0(X)$ that satisfies $F_0(R_{\min}) = F(R_{\min})$ and substitute this into the right-hand side of Eq. (45). We then solve Eq. (40) and choose the solution $B_\phi(X)$ that satisfies the boundary condition set by $F(R_{\min})$. Substituting $B_\phi(X)$ into the expressions for the remaining variables in Eq. (46) and

evaluating the right-hand side of Eq. (45) gives an iterated solution $F_1(X)$. We then substitute $F_1(X)$ back into the right-hand side and continue the iteration process until the solution converges.

B. Boundary layer

Outside the core region, the poloidal field terms in Eq. (30) become important, corresponding to the derivatives of ψ in Eq. (22) becoming large. Since the derivative perpendicular to the boundary is much larger than that parallel to the boundary, we introduce the variable ξ which is the perpendicular distance inward from the boundary and make the approximation $\nabla = \hat{\xi}(\partial/\partial\xi)$.[14,15] To lowest order, Eq. (22) becomes[14,15]

$$\frac{\partial}{\partial\xi}\left[(1-\Delta)\frac{\partial\psi}{\partial\xi}\right] = \mu_0\left[RJ_\phi(R,X) - XJ_{c\phi}(X)\right]. \tag{47}$$

The solution then follows analogously to Ref. 15 but with the additional factor of $1-\Delta$, giving

$$\frac{\partial\psi}{\partial\xi}(R,X) = \frac{\sqrt{-2\mu_0\Lambda(R,X)}}{1-\Delta(R,X)} \tag{48}$$

and

$$\xi(R,X) = \int_{R_{\min}}^{X} dX' \frac{(d\psi/dX')[1-\Delta(R,X')]}{\sqrt{-2\mu_0\Lambda(R,X')}}, \tag{49}$$

where

$$\Lambda(R,X) \equiv \int_X^R dX'' \frac{d\psi}{dX''}[1-\Delta(R,X'')]\left[RJ_\phi(R,X'') - X''J_{c\phi}(X'')\right]. \tag{50}$$

For all physical solutions, $R \geq X$ must be satisfied; the boundary layer solution approaches the core solution as $R \to X$.

To calculate ξ, we let $d\psi/dX$ be another free function of X. To understand the physical significance of this function, we note that the safety factor q in the core can be expressed to lowest order as[14]

$$q(X) = \frac{F(X)l(X)}{\pi X|d\psi/dX|}, \tag{51}$$

where $l(X)$ is half the length of the X surface in the core (which is approximately half the length of vacuum vessel due to the narrowness of the boundary layer). Therefore, with $F(X)$ already specified, $d\psi/dX$ determines the safety factor in the core.

The poloidal magnetic field B_θ in the boundary layer can be calculated from Eq. (48), since $B_\theta = |\nabla\psi \times \nabla\phi| = (\partial\psi/\partial\xi)/R$. However, the right-hand side of Eq. (48) is also dependent on $\partial\psi/\partial\xi$ through the B_θ dependence of Λ and Δ; therefore, we solve Eq. (48) iteratively for $\partial\psi/\partial\xi$, which we will describe in more detail below. We then substitute the converged values for the quantities in Eq. (48) into Eq. (49) to calculate ξ.

In the boundary layer B_ϕ is given by

$$B_\phi(R,X) = \frac{F(X)}{R[1-\Delta(R,X)]}, \tag{52}$$

where $F(X)$ is the solution of Eq. (45). We use $B^2 = B_\theta^2 + B_\phi^2$ and substitute Eqs. (7), (16)–(18), and (20) into Eq. (52) to calculate an eighth-order polynomial equation for $B(R,X)$

$$0 = R^2(B^2 - B_\theta^2)[B(B - T_\parallel\Theta)^2 + \tilde{Y}(R,X)T_\parallel^2\Theta]^2 - B^2(B - T_\parallel\Theta)^4F^2, \tag{53}$$

where

$$\tilde{Y}(R,X) = \frac{\mu_0 k}{m}\rho_i(X)\exp\left(\frac{m(R^2-X^2)\Omega^2}{2kT_\parallel}\right). \tag{54}$$

The appropriate solution of Eq. (53) is positive real and satisfies $B(R=X,X) = B_\phi(X)$ so that the magnetic field in the boundary layer matches the (purely toroidal) magnetic field in the core as $R \to X$.

The iteration for $\partial\psi/\partial\xi$ proceeds as follows. We first assume an initial function

$$\frac{\partial\psi}{\partial\xi}(\tilde{R},X) = \left(\frac{\partial\psi}{\partial\xi}\right)_0(\tilde{R},X), \tag{55}$$

for some $\tilde{R} \in [R_{\min}, R_{\max}]$ with $R_{\min} \leq X \leq \tilde{R}$, where

$$\left(\frac{\partial\psi}{\partial\xi}\right)_0(\tilde{R}, X=\tilde{R}) = 0, \tag{56}$$

to satisfy the boundary condition previously stated. For the first iteration step, we set

$$B_\theta = B_{\theta 0}(\tilde{R},X) \equiv \frac{(\partial\psi/\partial\xi)_0(\tilde{R},X)}{\tilde{R}}, \tag{57}$$

in Eq. (53) and solve numerically for $B(\tilde{R},X)$. We then substitute the appropriate solution for $B(\tilde{R},X)$ into the variables in Eq. (48) and compute the integral $\Lambda(\tilde{R},X)$; this gives us our updated function $(\partial\psi/\partial\xi)_1(\tilde{R},X)$. We continue the iteration procedure until convergence is achieved. The converged values are substituted into Eq. (49) to determine $\xi(\tilde{R},X)$. Finally, we repeat the calculation for regularly spaced values of $\tilde{R} \in [R_{\min}, R_{\max}]$ to obtain $\xi(R,X)$.

C. Plotting flux surfaces

With ξ obtained, we can now determine the high-β flux surfaces, which are contours of constant X. We follow the plotting method described in Ref. 14, in which the (R, Z) coordinates of these flux contours are calculated in two separate regions then joined. Away from $R = R_{\max}$, the Z position of a given X contour at R is given by

$$Z(R,X) = l(R) - \xi(R,X)\sqrt{1 + \left(\frac{dl(R)}{dR}\right)^2}. \tag{58}$$

Near $R = R_{max}$, the contours are more accurately calculated in terms of the distance between the plasma boundary and the flux surface. Using this approach, the coordinates of the X flux surface are given by

$$(R, Z) = (R_i + \Delta R, l(R_i) - \Delta Z), \tag{59}$$

for input values $R_i \leq R_{max}$, where

$$\Delta R(R_i, X) = \xi(R_i, X) \frac{dl(R_i)/dR_i}{\sqrt{1 + [dl(R_i)/dR_i]^2}}, \tag{60}$$

$$\Delta Z(R_i, X) = \xi(R_i, X) \frac{1}{\sqrt{1 + [dl(R_i)/dR_i]^2}}. \tag{61}$$

These two solutions are joined where the distance between them attains a minimum; this gives an accurate representation of the complete flux surface since there is an overlap region in which both solutions are accurate. The solution given by Eq. (58) asymptotes to the vertical line $R = X$ (i.e., the core solution), so the core solution is only used along the midplane, where $Z = 0$.

V. NUMERICAL IMPLEMENTATION

A. Core

We now numerically implement the analytical solution for the core region derived in Sec. IV A. To proceed we first choose particular functional forms for the free functions. As by Fitzgerald *et al.*,[15] we let the free functions $\Omega(X), T_\parallel(X)$, $\rho_i(X)$, and $\Theta(X)$ take the form

$$f(X) = f_0 \left(1 - \frac{(R_{max} - X)^2}{(R_{max} - R_{min})^2}\right), \tag{62}$$

for given inputs $f_0 = \{\Omega_0, T_{\parallel 0}, \rho_{i0}, \Theta_0\}$, so that the functions are maximal at $X = R_{max}$. In reality, the functions should be maximal at the magnetic axis R_{mag};[14] Eq. (62) is therefore a good approximation where the boundary layer is narrow and the Shafranov shift is large (see Fig. 1). We also let $d\psi/dX$ take the form

$$\frac{d\psi}{dX} = a_\psi l(X), \tag{63}$$

for a given input a_ψ (so that the safety factor in Eq. (51) remains finite at $X = R_{min}$ where $d\psi/dX = 0$) and assume a circular boundary

$$l(X) = \sqrt{(X - R_{min})(R_{max} - X)}. \tag{64}$$

The input values that we choose are listed in Table I, where m is the mass of deuterium. The value of ρ_{i0} is chosen to give an average toroidal beta $\beta_T \equiv 2\mu_0 \langle p \rangle / B_{T0}^2$ of 70% in the isotropic case (where $\langle p \rangle$ is the volume-averaged isotropic pressure and B_{T0} is the vacuum magnetic field at the geometric axis) to be close to values for proposed high-β experiments.

TABLE I. Input parameters chosen for the numerical calculation of equilibria.

Parameter	Value
R_{min}	0.1 m
R_{max}	1 m
ρ_{i0}	$m \times 3.5 \times 10^{20}\ \mathrm{m}^{-3}$
$kT_{\parallel 0}$	10 keV
a_ψ	1×10^{-3} T
$F(R_{min})$	0.6 Tm

1. Isotropic equilibria

We now present the results for isotropic ($\Theta_0 = 0$) high-β equilibria with and without flow. (These results are qualitatively the same as Ref. 15). A diamagnetic hole is identified as a region where the solution for $F(X)$ passes through zero and becomes imaginary, thus signifying an unphysical solution of the Grad-Shafranov equation. Using the values in Table I and varying ρ_{i0} we find that $\beta_T \geq 57\%$ for diamagnetic hole formation, so our calculations for $\beta_T = 70\%$ will have a diamagnetic hole. The flux function F and the magnetic field strength B in the core are graphed in Fig. 2 for different toroidal flow speeds determined by the parameter Ω_0. For no flow ($\Omega_0 = 0$), a diamagnetic hole exists in the region $0.83 \leq X \leq R_{max}$. The hole region becomes smaller as Ω_0 increases, with the left and right boundaries of the hole moving to larger and smaller X, respectively, and the diamagnetism is reduced. When $\Omega_0 = \Omega_{min} \equiv 2.91 \times 10^5\ \mathrm{s}^{-1}$, $F(X)$ and $B(X)$ are positive for all X, so the toroidal flow has suppressed the diamagnetic hole. (This flow speed corresponds to the normalized value $\Omega_{min} R_{max}/V_\parallel = 0.42$: i.e., the minimum tangential flow speed at R_{max} normalized by $V_\parallel = \sqrt{kT_{\parallel 0}/m}$, the parallel thermal speed at R_{max}.) For increasing Ω_0 above Ω_{min} the diamagnetism is further reduced and $F(X)$ asymptotes to its vacuum profile—i.e., $F(X) = F(R_{min})$ for all X—so that $B(X)$ asymptotes to the vacuum magnetic field $B_{vac}(X) = F(R_{min})/X$.

2. Anisotropic equilibria, $T_\parallel > T_\perp$

For our calculations of high-β equilibria with anisotropy and flow we vary the anisotropy through the parameter Θ_0. The equilibrium profiles of F, B, $T_\parallel/T_\perp$, and Δ without flow are graphed in Fig. 3 for different values of $\Theta_0 \leq 0$, corresponding to $T_\parallel \geq T_\perp$. We first choose a nominal value of $\Theta_0 = -1 \times 10^{-9}\ \mathrm{TK}^{-1}$ which gives $\max(T_\parallel/T_\perp) = 1.24$ (see Fig. 3(c)). Figure 3(b) shows that this level of anisotropy gives a solution with no diamagnetic hole. As Θ_0 becomes more negative than this nominal value, the diamagnetism is reduced; for large negative Θ_0, $F(X)$ and $B(X)$ approach their vacuum profiles.

As Θ_0 becomes less negative than the nominal value, the plasma diamagnetism becomes stronger and $\max(\Delta)$ increases; this continues until $\Theta_0 = \Theta_{min} \equiv -1.12 \times 10^{-10}\ \mathrm{TK}^{-1}$, corresponding to $\max(T_\parallel/T_\perp) = 1.07$, where we find $\max(\Delta) = 1$ at $X = R_{max}$ as shown in Fig. 3(d). We note from Fig. 3(b) that $B(X) = F(X)/[X(1 - \Delta(X)]$ remains finite as both $F(X)$ and $1 - \Delta(X)$ approach zero at $X = R_{max}$. For $\Theta_{min} < \Theta_0 < 0$, the

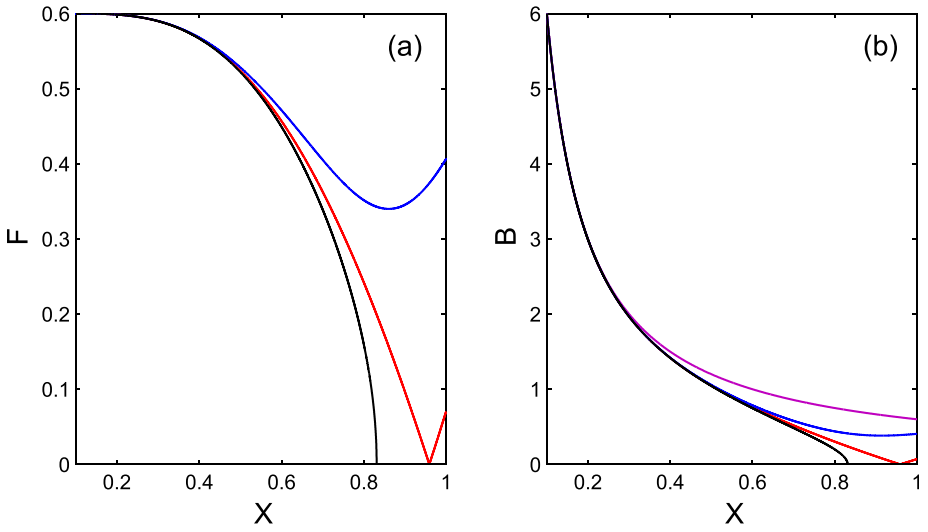

FIG. 2. Isotropic equilibrium profiles of (a) F and (b) B in the core for flow speeds $\Omega_0 = 0$ (black), $\Omega_0 = \Omega_{\min} \equiv 2.91 \times 10^5\ \mathrm{s}^{-1}$ (red), and $\Omega_0 = 5 \times 10^5\ \mathrm{s}^{-1}$ (blue). In (b), the vacuum magnetic field $B_{\mathrm{vac}}(X) = F(R_{\min})/X$ is graphed in purple.

"firehose condition" for equilibrium existence stated in Eq. (8) is violated and the equilibrium problem is no longer solvable. This manifests in the cubic equation for B in Eq. (40) no longer having at least one positive real solution for all X; instead, it has one negative solution and a pair of complex conjugate solutions near $X = R_{\max}$.

From these results, we see that all static ($\Omega_0 = 0$) equilibrium solutions with $T_\parallel > T_\perp$ suppress the diamagnetic hole found in static isotropic plasmas. Even a relatively weak anisotropy (i.e., $\max(T_\parallel/T_\perp) = 1.07$) produces such equilibrium solutions. The inclusion of a weak flow ($0 < \Omega_0 < \Omega_{\min}$) gives the same qualitative results but allows solutions for yet weaker anisotropy, as shown in Fig. 4. For $\Omega_0 > \Omega_{\min}$, solutions exist for all $\Theta_0 < 0$ and do not have a diamagnetic hole.

Plasmas with different β_T values require different levels of flow and anisotropy for no-hole solutions. In Fig. 5, we graph the minimum values of flow (for $\Theta_0 = 0$) and anisotropy (for $\Omega_0 = 0$) that give no-hole solutions for different β_T values. For $\beta_T = 60\%$ only a very small anisotropy of $\max(T_\parallel/T_\perp) = 1.01$ is required to satisfy the firehose condition (and thus give no-hole solutions) in static plasmas. We

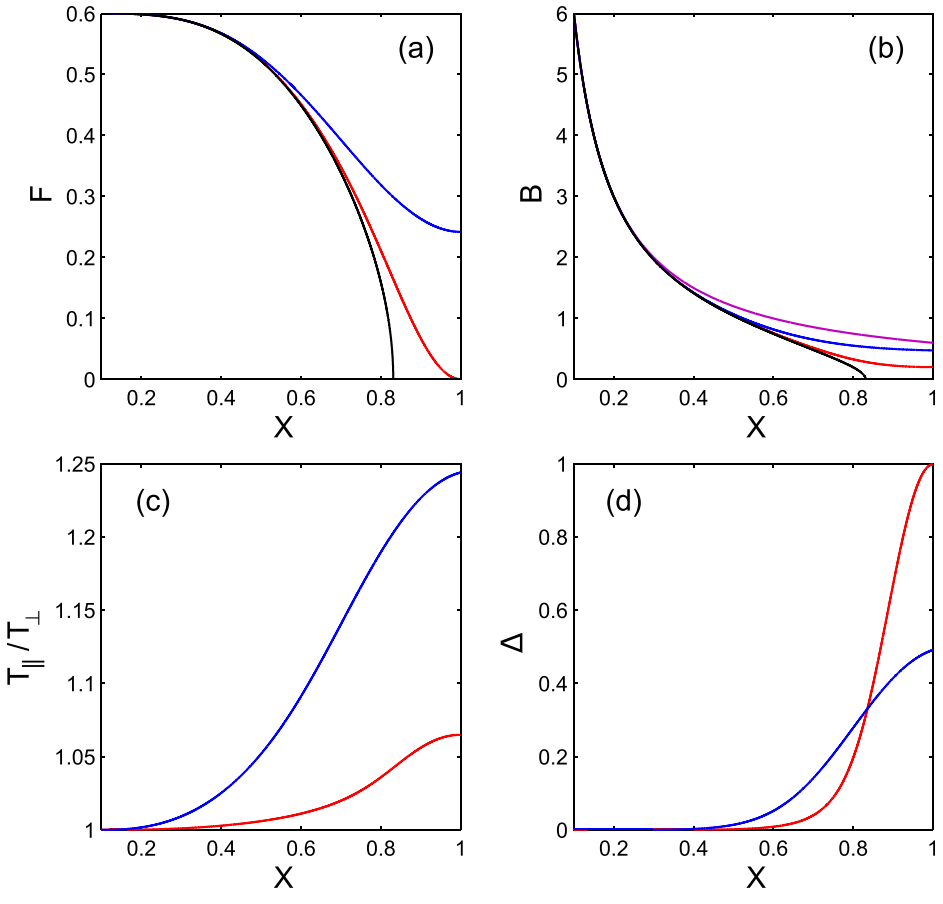

FIG. 3. Static ($\Omega_0 = 0$) equilibrium profiles in the core for $\Theta_0 = 0$ (black), $\Theta_0 = \Theta_{\min} \equiv -1.12 \times 10^{-10}\ \mathrm{TK}^{-1}$ (red), and $\Theta_0 = -1 \times 10^{-9}\ \mathrm{TK}^{-1}$ (blue).

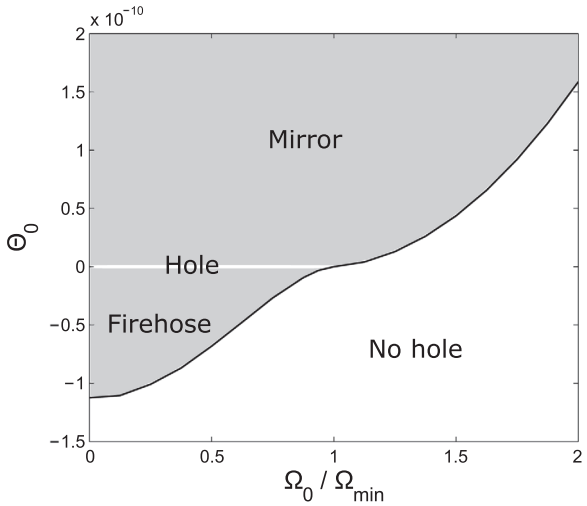

FIG. 4. Equilibrium solution regions in Ω_0-Θ_0 space for $\beta_T = 70\%$, with the boundary between the regions calculated quantitatively. The gray shaded region has no solution due to the violation of either the firehose or mirror condition; excluded from this region is the unshaded line at $\Theta_0 = 0$ for $\Omega_0/\Omega_{\min} < 1$ where a diamagnetic hole exists. In the remaining unshaded region, equilibrium solutions exist and have no diamagnetic hole.

note that even for $\beta_T = 100\%$ the required level of anisotropy in static plasmas is $\max(T_\parallel/T_\perp) = 1.23$, which is achievable using neutral beam injection.

3. Anisotropic equilibria, $T_\parallel < T_\perp$

We now calculate the equilibrium quantities for $\Theta_0 > 0$ (i.e., $T_\parallel < T_\perp$). Figure 6 shows the equilibrium profiles of F, B, $T_\parallel/T_\perp$, and $\tilde{\beta} \equiv \beta_\perp^2/\beta_\parallel - \beta_\perp$ for $\Omega_0 = 1 \times 10^6\,\mathrm{s}^{-1}$; this flow speed is greater than $\Omega_{\min}$ so there is no diamagnetic hole in the isotropic case. As Θ_0 increases, the diamagnetism becomes stronger, as shown for $\Theta_0 = 5 \times 10^{-10}\,\mathrm{TK}^{-1}$ corresponding to $\min(T_\parallel/T_\perp) = 0.93$. At $\Theta_0 = \Theta_{\max} \equiv 8.67 \times 10^{-10}\,\mathrm{TK}^{-1}$ (giving $\min(T_\parallel/T_\perp) = 0.85$), $\max(\tilde{\beta}) = 1$ at $X = 0.76$. For $\Theta_0 > \Theta_{\max}$ the "mirror condition" for equilibrium existence stated in Eq. (9) is violated, so there are no equilibrium solutions.

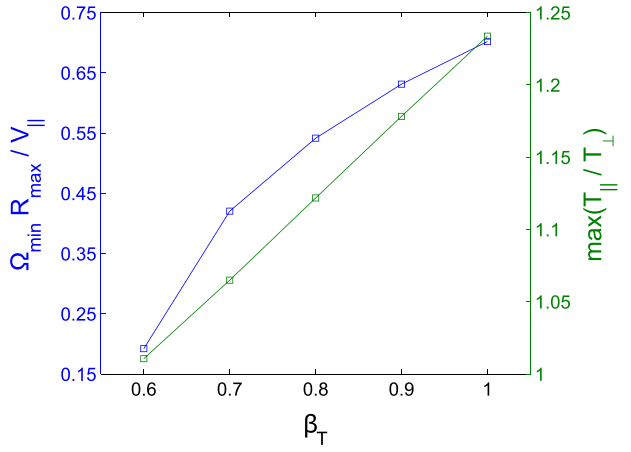

FIG. 5. Minimum flow speed and anisotropy required for no-hole solutions in isotropic and static plasmas, respectively, as a function of β_T. The minimum flow speed, graphed in blue, is quantified by $\Omega_{\min} R_{\max}/V_\parallel$: i.e., the minimum tangential flow speed at $R_{\max}$ normalized by $V_\parallel = \sqrt{kT_{\parallel 0}/m}$, the parallel thermal speed at $R_{\max}$. The minimum anisotropy, graphed in green, is quantified by $\max(T_\parallel/T_\perp)$.

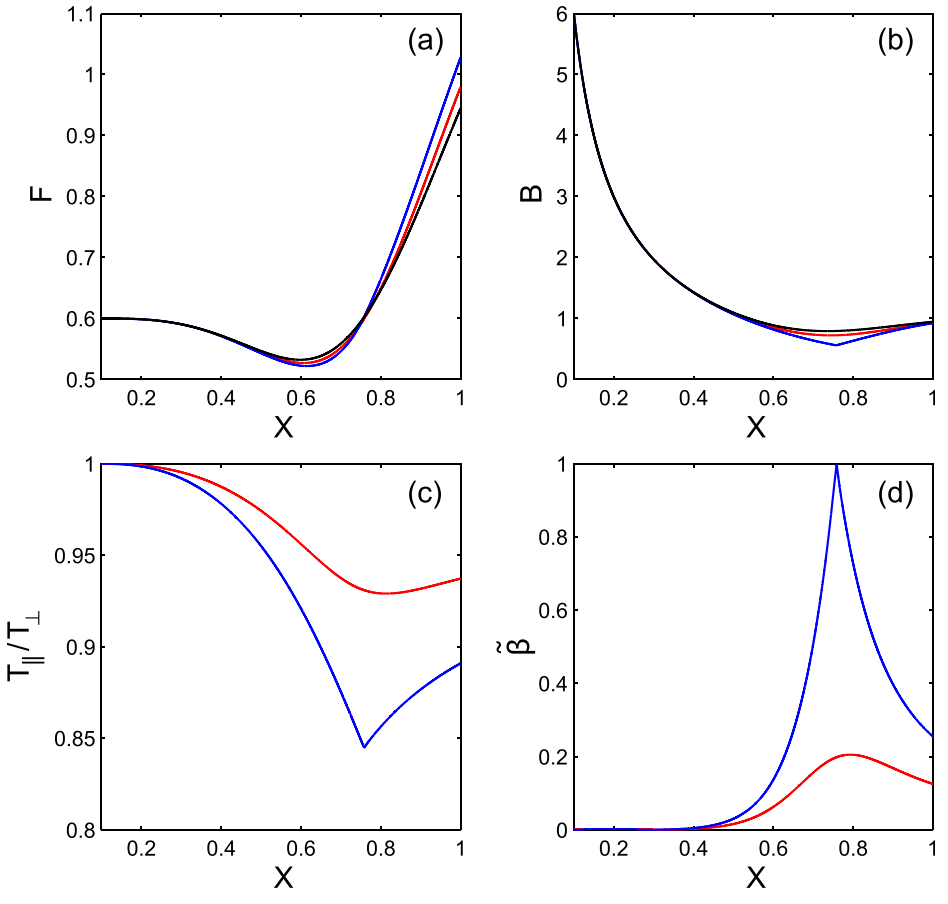

FIG. 6. Flowing ($\Omega_0 = 1 \times 10^6\,\mathrm{s}^{-1}$) equilibrium profiles in the core for $\Theta_0 = 0$ (black), $\Theta_0 = 5 \times 10^{-10}\,\mathrm{TK}^{-1}$ (red), and $\Theta_0 = 8.67 \times 10^{-10}\,\mathrm{TK}^{-1}$ (blue).

Stronger (weaker) toroidal flows still satisfying $\Omega_0 > \Omega_{\min}$ give the same qualitative results, but increase (decrease) the equilibrium-existence region, as shown in Fig. 4. For $\Omega_0 < \Omega_{\min}$ (where a diamagnetic hole exists for isotropic plasmas), we find that there are no equilibrium solutions.

4. Robustness to the choice of $\Theta(X)$

Numerical results from Secs. V A 2 and V A 3 show that the diamagnetic hole does not exist at *any* level of anisotropy (measured by Θ_0) for the $\Theta(X)$ profile given by Eq. (62); either a solution exists with no diamagnetic hole or no solution exists, as illustrated in Fig. 4. The non-existence of diamagnetic holes in the presence of anisotropy occurs not only for this choice of $\Theta(X)$ profile but also for any $\Theta(X)$ that is either positive or negative for all X. This can be seen through Eq. (16): for $\Theta(X) > 0$, $T_\perp/T_\parallel$ increases as B decreases, and approaches infinity at $B = T_\parallel\Theta$ which will lead to violation of the mirror condition for equilibrium existence; for $B < T_\parallel\Theta$ there is no valid solution since this gives $T_\perp < 0$. For $\Theta(X) < 0$, $B = 0$ is obtained only in the unphysical case of $T_\perp = 0$ (with non-zero $T_\parallel$). Thus, any non-zero level of anisotropy occurring throughout the plasma volume deletes the diamagnetic hole. If $\Theta(X)$ were to vanish in some region, corresponding to a region of perfect isotropy, the diamagnetic hole may reappear. However, it is not possible to find such a solution using our iterative method for Eq. (45). Unlike the isotropic case in which a region of imaginary $F(X)$ can be immediately identified as the hole region, a trial solution $F_n(X)$ of Eq. (45) that is imaginary in some region will generate a complex updated solution $F_{n+1}(X)$, leading to continual changes to the unphysical solution region during the updating procedure and thus convergence cannot be achieved.

B. Boundary layer

The analytical solution for the boundary layer derived in Sec. IV B is numerically implemented in this section using the parameters in Table I. The complete flux surfaces are graphed in Fig. 7 for static equilibria with $\Theta_0 = 0$ and $\Theta_0 = -1 \times 10^{-9}\,\mathrm{TK}^{-1}$. The $\Theta_0 = 0$ (isotropic) graph shows the strongly outward-shifted D-shaped flux surfaces familiar from previous work,[13–15] with a diamagnetic hole for $0.83 \le X \le 0.97$. We find that the boundary layer width increases as Θ_0 becomes more negative; for no-hole solutions, in which the magnetic axis is a well defined entity, the wider boundary layer necessarily results in a smaller Shafranov shift.

For $\Theta_0 > 0$ and Ω_0 not much greater than $\Omega_{\min}$, we find that the boundary layer width decreases relative to the isotropic case for the same flow speed, and we expect the same result for larger Ω_0. However, both the isotropic and anisotropic boundary layer solutions begin to break down near $R = R_{\max}$ as Ω_0 increases further above $\Omega_{\min}$. That the solutions break down is evident because $\Lambda(R, X')$ in Eq. (49) becomes positive, thus ξ becomes imaginary. The domain of validity of the boundary layer solutions is reduced to smaller R as Ω_0 increases. We find that an accurate representation of the flux surfaces can still be obtained when $\Omega_0/\Omega_{\min} \lesssim 3$ by interpolation at large R with semicircular contours.

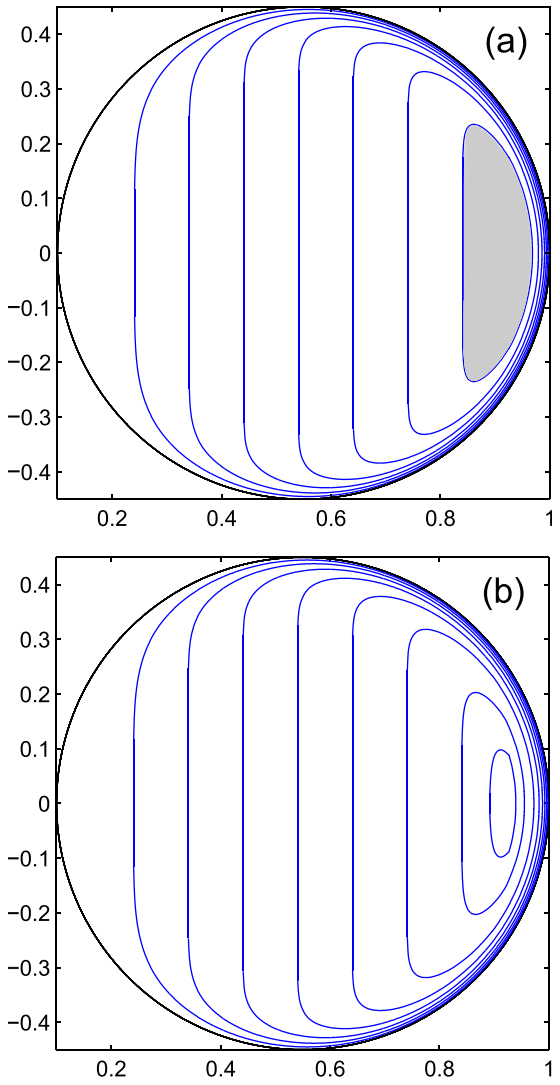

FIG. 7. Contours of constant poloidal magnetic flux ψ for (a) $\Theta_0 = 0$ and (b) $\Theta_0 = -1 \times 10^{-9}\,\mathrm{TK}^{-1}$, with $\beta_T = 70\%$.

VI. CONCLUSION

We have extended previous analytical calculations of 2D high-β equilibria in order-unity aspect ratio tokamaks with toroidal flow to include pressure anisotropy, by solving a modified Grad-Shafranov equation in the core and boundary layer regions. Our calculations are based on the guiding-center plasma model for a bi-Maxwellian distribution (with parallel temperature as a flux function), the ideal MHD Ohm's law, and approximations of the force-balance equations valid for the orderings $\beta q^2 \gg \epsilon^2$ and $M_\phi^2 q^2 \gg \epsilon$. These assumptions are not unreasonable for a future high-β tokamak.

We find that pressure anisotropy with $p_\parallel > p_\perp$ ($p_\parallel < p_\perp$) reduces (enhances) the plasma diamagnetism relative to the isotropic case whenever an equilibrium solution exists, which occurs if and only if the firehose (mirror) condition is satisfied.

Calculations with our model give no anisotropic equilibria with diamagnetic holes (which exist in the isotropic case

for $\Omega_0 < \Omega_{min}$). For $\beta_T = 70\%$, equilibria exist for $\max(p_\parallel/p_\perp) > 1.07$. Hence, even a weak anisotropy gives equilibrium solutions with no hole. Conversely, for $p_\parallel < p_\perp$ there are no equilibrium solutions below Ω_{min}, while above Ω_{min} equilibrium solutions with no hole may exist for sufficiently weak anisotropy. The boundary layer width increases and the Shafranov shift decreases for $p_\parallel > p_\perp$, while the converse is true for $p_\parallel < p_\perp$.

ACKNOWLEDGMENTS

This work was funded by the Australian Research Council through Grant Nos. DP140100790 and FT0991899.

[1]M. Ono and R. Kaita, Phys. Plasmas **22**, 040501 (2015).
[2]M. Gryaznevich, R. Akers, P. G. Carolan, N. J. Conway, D. Gates, A. R. Field, T. C. Hender, I. Jenkins, R. Martin, M. P. S. Nightingale, C. Ribeiro, D. C. Robinson, A. Sykes, M. Tournianski, M. Valovic, and M. J. Walsh, Phys. Rev. Lett. **80**, 3972 (1998).
[3]D. A. Gates and NSTX National Research Team, Phys. Plasmas **10**, 1659 (2003).
[4]Y.-K. M. Peng, P. J. Fogarty, T. W. Burgess, D. J. Strickler, B. E. Nelson, J. Tsai, C. A. Neumeyer, R. Bell, C. Kessel, J. Menard, D. Gates, B. LeBlanc, D. Mikkelsen, E. Fredrickson, L. Grisham, J. Schmidt, P. Rutherford, S. Sabbagh, A. Field, A. Sykes, I. Cook, O. Mitarai, and Y. Takase, Plasma Phys. Controlled Fusion **47**, B263 (2005).
[5]F. Najmabadi, M. Billone, L. Bromberg, V. Chan, F. Dahlgren, D. A. Deuser, L. A. El-Guebaly, H.-M. Fan, S. C. Jardin, H. Y. Khater, C. E. Kessel, L. Lao, Y. R. Linliu, S. Malang, T. K. Mau, J. Menard, R. Miller, R. L. Miller, E. A. Mogahedi, C. Neumeyer, T. Petrie, P. Politzer, S. Pourrahimi, J. Pulsifer, W. Reiersen, J. H. Schultz, K. T. Slattery, R. D. Stambaugh, D. Steiner, I. Sviatoslavsky, D. K. Sze, M. S. Tillack, P. Titusf, A. D. Turnbull, X. R. Wang, L. M. Waganer, G. W. Wille, I. Zatz, and ARIES Team, Fusion Eng. Des. **65**, 143 (2003).
[6]H. Wilson, J.-W. Ahn, R. Akers, D. Applegate, R. Cairns, J. Christiansen, J. Connor, G. Counsell, A. Dnestrovskij, W. Dorland, M. Hole, N. Joiner, A. Kirk, P. Knight, C. Lashmore-Davies, K. McClements, D. McGregor, M. O'Brien, C. Roach, S. Tsaun, and G. Voss, Nucl. Fusion **44**, 917 (2004).
[7]R. Iacono, A. Bondeson, F. Troyon, and R. Gruber, Phys. Fluids B **2**, 1794 (1990).
[8]L. Guazzotto, R. Betti, J. Manickam, and S. Kaye, Phys. Plasmas **11**, 604 (2004).
[9]M. Hole, G. Von Nessi, M. Fitzgerald, K. McClements, J. Svensson, and MAST Team, Plasma Phys. Controlled Fusion **53**, 074021 (2011).
[10]M. Fitzgerald, L. C. Appel, and M. J. Hole, Nucl. Fusion **53**, 113040 (2013).
[11]Z. S. Qu, M. Fitzgerald, and M. J. Hole, Plasma Phys. Controlled Fusion **56**, 075007 (2014).
[12]A. Ivanov, A. Martynov, S. Medvedev, and Y. Poshekhonov, Plasma Phys. Rep. **41**, 203 (2015).
[13]S. C. Cowley, P. K. Kaw, R. S. Kelly, and R. M. Kulsrud, Phys. Fluids B **3**, 2066 (1991).
[14]S. C. Hsu, M. Artun, and S. C. Cowley, Phys. Plasmas **3**, 266 (1996).
[15]M. Fitzgerald, S. Sharapov, and M. Hole, Phys. Plasmas **18**, 092508 (2011).
[16]R. Y. Neches, S. C. Cowley, P. A. Gourdain, and J. N. Leboeuf, Phys. Plasmas **15**, 122504 (2008).
[17]H. Grad, Proc. Symp. Appl. Math. **18**, 162 (1966).
[18]H. Grad, Phys. Fluids **10**, 137 (1967).
[19]D. Dobrott and J. M. Greene, Phys. Fluids **13**, 2391 (1970).
[20]D. J. Southwood and M. G. Kivelson, J. Geophys. Res. **98**, 9181, doi:10.1029/92JA02837 (1993).
[21]J. P. Goedbloed, R. Keppens, and S. Poedts, *Advanced Magnetohydrodynamics: With Applications to Laboratory and Astrophysical Plasmas* (Cambridge University Press, Cambridge, 2010).